SCIENCE CHINA
Chemistry

•ARTICLES•

February 2020 Vol.63 No.2: 208–214
https://doi.org/10.1007/s11426-019-9632-2

A C_2-symmetric triple [5]helicene based on *N*-annulated triperylene hexaimide for chiroptical electronics

Zetong Ma[1,4], Thorsten Winands[3], Ningning Liang[2], Dong Meng[1], Wei Jiang[1,4*], Nikos L. Doltsinis[3*] & Zhaohui Wang[1,2*]

[1]*CAS Research/Education Center for Excellence in Molecular Sciences, Institute of Chemistry, Chinese Academy of Sciences, Beijing 100190, China;*
[2]*Key Laboratory of Organic Optoelectronics and Molecular Engineering, Department of Chemistry, Tsinghua University, Beijing 100084, China;*
[3]*Institute for Solid State Theory and Center for Multiscale Theory & Computation, University of Muenster, Wilhelm-Klemm-Strasse 10, Muenster 48149, Germany;*
[4]*University of Chinese Academy of Sciences, Beijing 100049, China*

Received July 28, 2019; accepted October 9, 2019; published online November 14, 2019

Two diastereoisomers (NTPH-P and NTPH-T1) as a C_2-symmetric triple [5]helicene based on *N*-annulated triperylene hexaimide were synthesized. Aided by nuclear magnetic resonance spectroscopy (NMR) and theoretical calculations, NTPH-P was assigned to three-blade propeller conformation while NTPH-T1 tended to exhibit twisted conformation with pyrrole ring fusing on a bowl-shaped PDI foil. Characterized by circular dichroism (CD) and circular polarized luminescence (CPL) measurements, the enantiomerically pure NTPH-P exhibited fairly good chiral activities both in the absorption and emission range with dissymmetry factors $|g_{abs}|$ of 4.1×10^{-3} and $|g_{lum}|$ of 1.2×10^{-3}. The diastereoisomers were further employed as acceptors for organic solar cells with distinct PCEs of 8.11% and 5.24% for NTPH-P and NTPH-T1 based devices, respectively, signifying the prospects in chiroptical electronics by designing molecularly defined aromatics.

triple helicenes, perylene diimides, *N*-annulation, asymmetric decoration, chiroptical properties, organic solar cells

Citation: Ma Z, Winands T, Liang N, Meng D, Jiang W, Doltsinis NL, Wang Z. A C_2-symmetric triple [5]helicene based on *N*-annulated triperylene hexaimide for chiroptical electronics. *Sci China Chem*, 2020, 63: 208–214, https://doi.org/10.1007/s11426-019-9632-2

1 Introduction

Curved polycyclic aromatics with extended π-structures have sparked increasing attention in materials science due to their peculiar topology and electronic properties along with good stability and processibility [1–6]. It is still a challenge to design molecularly defined aromatics with large and curved skeleton because of the difficulties in precisely synthesizing such crowded molecules and fully exalting their properties [7]. Helicenes present an important class of curved molecules with helical chirality induced by van der Waals repulsion of *ortho*-fused rings [8]. Till now, a restricted number of helical systems with stable enantiomers have been described, and the purely enantiomeric properties, such as their chiroptical, optoelectronic, and supramolecular properties, is far underexplored [9–11]. To this end, plural helicities by accumulation of more helical substructures, as exemplified by double to hexapole subhelicenes fused together, have been being reported [12–26].

In this context, we have recently designed a triple [5]helicene, namely triperylene hexaimides (**3**, TPH), by jointing

*Corresponding authors (email: jiangwei@iccas.ac.cn; nikos.doltsinis@wwu.de; wangzhaohui@mail.tsinghua.edu.cn)

three perylene diimides (PDIs) on a benzene centre, which is a C_3-symmtrically propeller-shaped molecule [27]. In view of the three blades of [5]helicene in the TPH stereostructure, there should theoretically exist two pairs of enantiomers involving four diastereoisomers. However, just one pair of propeller-shaped enantiomers was found without other twisted conformations in the obtained single crystals, and the subsequent resolution of corresponding racemates was proved to be difficult by standard chiral high-performance liquid chromatography (HPLC), probably due to lower isomerization barriers between enantiomers resulting from the high C_3-symmetry structure.

In the present strategy, we integrated a pyrrole ring into one of the three blades of TPH at the *bay*-region of the PDI unit to reduce the configurable symmetry from C_3 to C_2 (Figure 1). The resulting *N*-doped triperylene hexaimide (**5**, NTPH) not only maintains a triple [5]helicene structure, but also exhibits the following characteristics: (1) a more twisted and bowl-shaped structure produced by pyrrole incorporation because of the smaller N atom radius resulting in a shorter C–N bond; (2) increased solubility by additional alkylation on the pyrrole ring, further benefiting the chiral resolution of enantiomers and also fine-tuning the molecular assembly if used in optoelectronic devices; (3) well-tunable energy level donated by *N*-heterocyclic annulation for obtaining higher parameters in the optoelectronic devices; (4) clearer configuration differentiated by the reduced configurable symmetry. As expected, the combination of multiple helicities and asymmetric decoration for constructing C_2-symmetric triple [5]helicenes (**5**, NTPH) produced two diastereoisomers differing by the way the three peripheral PDI foils intertwined, namely NTPH-P (**5a**) and NTPH-T1 (**5b**), respectively. Their structures were verified by the experimental and theoretical supports. NTPH-P can be further optically resolved into two excellently stable pure enantiomers which exhibit fairly good chiral activities with impressive dissymmetry factors of $|g_{abs}|=4.1\times10^{-3}$ and $|g_{lum}|=1.2\times10^{-3}$. More importantly, NTPH-P produced a power conversion efficiency of up to 8.11%, a much higher photovoltaic performance than its stereoisomer (NTPH-T1: PCE=5.24%) when employing them as electron acceptors in polymer solar cells.

2 Results and discussion

2.1 Materials synthesis and characterization

The synthesis of NTPH **5** started from parent TPH **3**, a C_3-symmetric molecule composed of three PDI subunits fusing a central benzene ring, which was prepared by threefold Suzuki coupling reaction and subsequent I_2-catalyzed photocyclization. As shown in Scheme 1, the nitrogen-heterocyclic annulated TPH (**4**) was efficiently synthesized by two

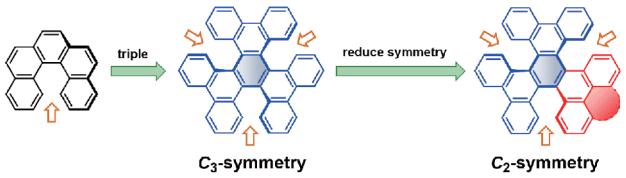

Figure 1 The strategy to design the C_2-symmetric triple [5]helicene (color online).

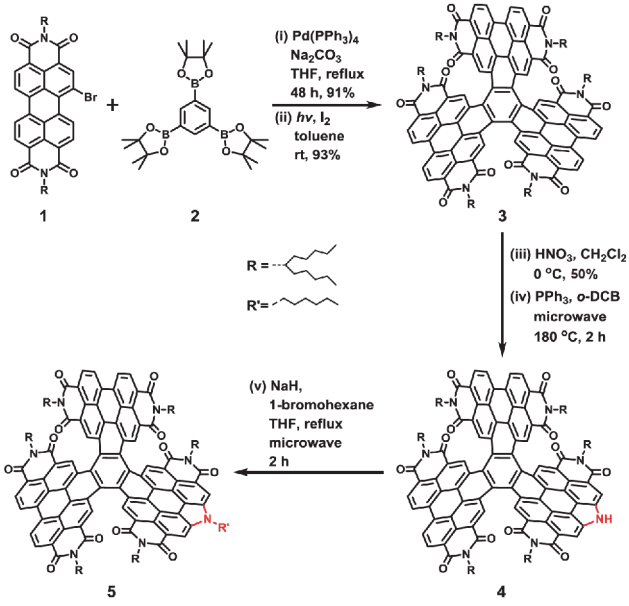

Scheme 1 The synthetic route to NTPH **5**. The cadogan reaction generated **4a** (yields: 38%) and **4b** (yield: 41%) in one pot; and the yields of compounds **5a** and **5b** from **4a** and **4b** are 91% and 93%, respectively (color online).

steps of regiospecifically electrophilic mononitration of TPH in an ice bath and subsequent microwave-assisted cadogan reaction with triphenylphosphine (PPh_3) in *o*-DCB [28,29]. Two fractions were easily separated and purified by column chromatography on silica gel in overall yields of 79% (38% yield for the first fraction **4a** and 41% yield of the second fraction **4b**) from the mononitrated TPH. Thus, the two compounds were then respectively converted to alkylated products NTPH in high yields for 91% for **5a** as dark-red solids and 93% for **5b** orange-red solids, respectively, treated with NaH and 1-bromhexane in THF by microwave radiation for 2 h. The compounds **5a** and **5b** produced primarily in the reaction are proven to be the diastereoisomers with the same isotropic distribution by high-resolution matrix assisted laser desorption lonization-time of flight (MALDI-TOF) high-resolution mass spectra (HRMS) shown in Figure S1 (Supporting Information online), although there should be three pairs of stereoisomers due to the lowered symmetry and the location of the pyrrole ring depicted in Figure 2. Both of them are freely soluble at room temperature in various organic solvents as a result of their contorted molecular scaf-

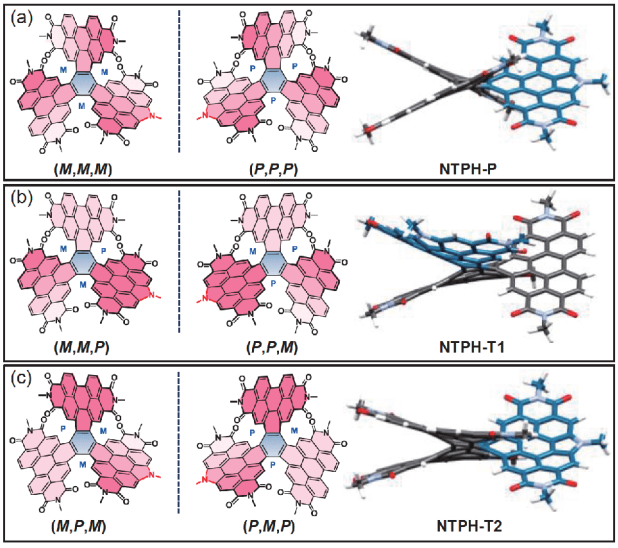

Figure 2 The six theoretical stereoisomers of NTPH-P (a), NTPH-T1 (b) and NTPH-T2 (c), and their corresponding optimized geometries calculated at PBE0/6-31 G* level. All long alkyl chains are replaced by methyl groups to speed up the calculations (color online).

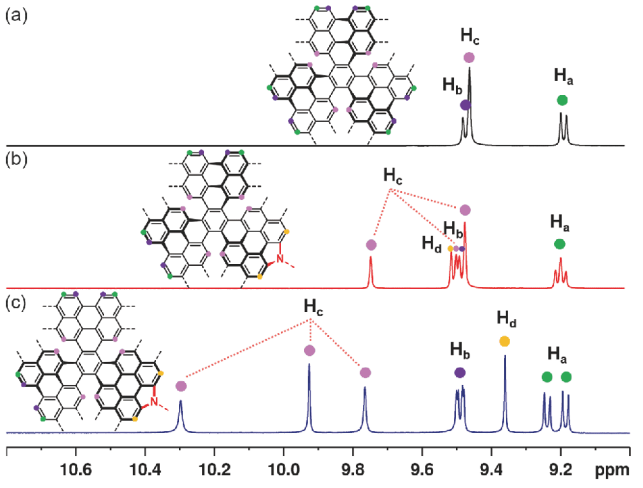

Figure 3 The ^{1}H NMR spectra of TPH (a), **5a** (b), and **5b** (c) at 373 K (color online).

fold and solubilizing chains on the imide positions and pyrrole rings. We have been unable to cultivate the crystal of NTPH with sufficient quality for single crystal structure determination by X-ray diffraction analysis, so we performed various nuclear magnetic resonance (NMR) measurement combined with quantum-chemical calculations of optimized geometries, electronic structure, and optical spectra to assist the identification of the two diastereoisomers.

The equilibrium structures of model NTPH with all alkyl chains replaced by methyl groups calculated by density functional theory (DFT) are shown in Figure 2. The difference between the diastereoisomers NTPH-P and NTPH-T lies in the way that their three peripheral PDI foils are intertwined. In Figure 2(a), NTPH-P presents a three-blade propeller conformation with an almost planar aromatic core of each PDI moiety. Two PDI subunits in NTPH-T exhibit a shallow bowl-shaped conformation facing in opposite directions, while the third PDI, exhibiting an almost-planar shape, lies between the other two PDI moieties. NTPH-T1 and NTPH-T2 differ on the location of the pyrrole ring in different PDI substructures. In NTPH-T1, the pyrrole ring is located at the bowl-shaped PDI moiety enhancing the curvature of the structure (Figure 2(b)), while the pyrrole ring is fused with the planar PDI unit in NTPH-T2. Compared with the bay regions torsion angles around the benzene core in TPH (25.10°, 26.96°, 32.97°), larger torsion angles occur in NTPH-P (28.62°, 28.63°, 30.54°) due to fusing the pyrrole ring in one PDI subunits. Owing to the twisted conformation, NTPH-T1 (28.06°, 29.75°, −35.00°) and NTPH-T2 (28.56°, 28.48°, −34.46°) show larger torsional angles (Figure S17).

Figure 3 shows the ^{1}H NMR spectra of TPH as well as two as-obtained NTPH diastereoisomers (**5a** and **5b**), in which the protons of H_a, which are split into doublets, were assigned to be the *nonbay* protons of the PDI core by the ^{1}H-^{1}H COSY and heteronuclear multiple bond correlation (HMBC) spectra. Because of reduced molecular symmetry and different stereo-configuration, the four H_a protons exhibit different splittings in **5a** and **5b**, two overlapping doublets and a two separated doublets, respectively. Additionally, the ^{1}H-^{1}H COSY spectra and the identical coupling constants revealed the correlation between H_a and H_b, and thus assigned H_b to the protons of the *bay* regions as no correlation with the carbonyl carbon was found by heteronuclear multiple bond correlation (HMBC) spectra (Figures S2–S5).

As the HMBC signals for carbon nuclei of peripheral *bay*-position in the pyrole-fused PDI unit coexisted in both protons on the first methylene of the pyrrole's alkyl chain and peripheral *ortho* protons, H_d was assigned to the proton of the peripheric *nonbay* region in the pyrole-fused PDI unit (Figure S8). The result was futher verified by the ^{1}H-^{1}H nuclear overhauser effect spectroscopy (NOESY) spectra (Figure S9). Analogously, as for **5b**, H_d at 9.36 ppm was assigned to the proton of the peripheric *nonbay* region in the pyrole-fused PDI unit by HMBC spectra (Figure S10), while the remaining ones (H_c) are hydrogens on the inward *nonbay* position. As shown, the inward *nonbay* hydrogens for **5a** (δ=9.74, 9.49 and 9.46 ppm) and **5b** (δ=10.30, 9.93 and 9.76 ppm) behaved differently, and thus were suitable for stereostructure analysis via NOESY spectra. For model NTPH-P, the inner *ortho* protons, divided into three classes, possessed no more than one reponse in the ^{1}H-^{1}H NOESY spectra (Figure S11). Expectedly, just one signal showed between protons at 9.74 and 9.49 ppm for **5a**. Moreover, ^{1}H NMR spectra in the aryl region for **5a** was considerably similar to the one for TPH 3. Therefore, the results above suggested a predominant propeller configuration as model

NTPH-P for **5a**. According to the theoretical structures for twisted conformation, it indicated that just a single NOESY signal exists for NTPH-T2, while more than one response was obtained for NTPH-T1 because all the inward hydrogens were located in inequivalent chemical environments. In the selective excitation NOESY spectra (Figure S12), hydrogens at 9.76 ppm showed NOE correlation with protons at 9.93 and 10.30 ppm with different response signal strengths, indicating the inward protons possessed at least two kinds of spatial correlation with different spatial separations between the protons. As a consequence, the aforementioned theoretical (Figure S18) and experimental results suggest that compound **5b** has a twisted configuration like model NTPH-T1. In contrast to the chemical signals of inward positions of PDI subunits (H_c) for **5a**, the protons for **5b** appear downfield in the NMR spectra, suggesting an enhanced deshielding effect of the twisted conformation probably caused by enlarged dihedral angles of the PDI moieties [21,30].

2.2 Optical and electrochemical properties

The calculated and experimental absorption spectra of the related compounds NTPH-P and NTPH-T1 are depicted in Figure 4. Both of these two compounds display broad absorption in the region of 300–600 nm. For the absorption spectra of **5a**, a shoulder peak at 556 nm is observed in addition to an intense absorption maximum at 524 nm (92,620 M^{-1} cm^{-1}) and a less intense peak at 498 nm (Table 1). By contrast, compound **5b** gave similar but hypsochromically-shifted absorption bands with a weak shoulder peak at 537 nm and a less intense peak at 505 nm and an intense peak at 476 nm (96,500 M^{-1} cm^{-1}). Analogously, the calculated ultraviolet-visible spectroscopy (UV-Vis) also demonstrated similar characteristics, which further supports our assignment of **5a** and **5b** to the proposed calculated NTPH-P and NTPH-T1 conformation, respectively. The time-dependent density-functional theory (TDDFT) calculations clarify the differences of spectra between NTPH-P and NTPH-T1. Analysis of the TDDFT eigenvectors reveals that in the absorption spectrum of NTPH-P (Figure S19(a) and Table S1, Supporting Information online), the lowest energy band at 556 nm can be assigned to the S_0-S_1 excitation primarily involving a highest occupied molecular orbital (HOMO)→lowest unoccupied molecular orbital (LUMO) transition. The absorption band at 524 nm is attributed to the S_0-S_3 excitation with a oscillator strength of 0.9558 and strong contributions of the HOMO→LUMO+1 transition and HOMO-1→LUMO transitions. And the high energy peaks from 350 to 400 nm predominantly involve electronic transition from the HOMO-2, HOMO-1, and HOMO to the LUMO+4 and LUMO+3. For the twisted molecule NTPH-T1, the lowest-energy maximum at 537 nm is dominated by a HOMO→LUMO excitation. The following maximum at 505 nm is mainly attributed to the S_0-S_2 transition dominated by a HOMO-1 to LUMO+1 excitation, and the crest at 476 nm is due to the transition from HOMO-1 to LUMO+2 (Figure S19(b)). The calculated energy levels and absorption spectra revealed that the changes in geometry can lead to a reordering of the frontier orbitals and differences in excitation characteristics in the two isomers. As a result, smaller electron excitation energies were observed in compound **5a**, resulting in a red-shifted absorption region compared with **5b**. From the cyclic voltammograms for compound **5a** and **5b** shown in Figure S14, the LUMO levels in CH_2Cl_2 solution are determined to be −3.79 and −3.77 eV, respectively. Both LUMO levels are higher than that of TPH (−3.83 eV) because of the electron-rich pyrrole ring and the electron donating effect of long *n*-hexyl chain. Both the calculated and experimental energy levels for these two isomers show

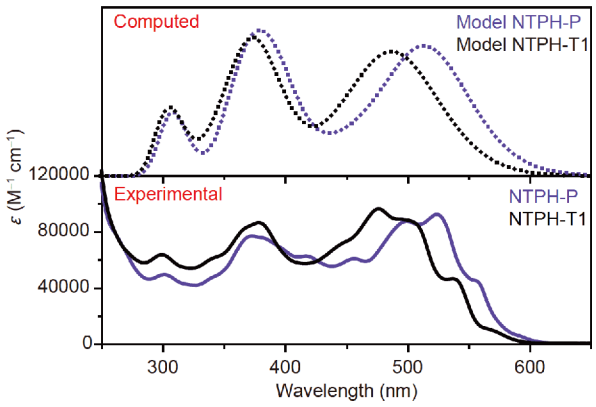

Figure 4 Top: theoretical absorption spectra of NTPH-P and NTPH-T1 with a Lorentzian line width of 1,300 cm^{-1} calculated at the TDDFT/PBE0/6-31G* level; bottom: experimental absorption spectra of NTPH-P and NTPH-T1 in $CHCl_3$ (10^{-5} M) (color online).

Table 1 Optical and electrochemical properties of **3** (TPH), **5a** (NTPH-P) and **5b** (NTPH-T1)

	λ_{abs} [a] (nm)	ε_{max} [a] (M^{-1} cm^{-1})	λ_{onset} [a] (nm)	λ_{em} [a] (nm)	Φ_{fl} [a] (%)	E_{1r} [b] (eV)	E_{2r} [b] (eV)	E_{LUMO} [c] (eV)	E_{HOMO} [d] (eV)	E_g [e] (eV)
3	486, 516	159,007	566	602	13.0	−1.12	−1.27	−3.83	−6.02	2.19
5a	498, 524, 556	92,620	579	608	10.9	−1.14	−1.22	−3.79	−5.93	2.14
5b	476, 505, 537	96,500	561	597	27.4	−1.18	−1.26	−3.77	−5.98	2.21

a) λ_{abs}, ε_{max}, λ_{onset}, λ_{em} and Φ_{fl} were measured in $CHCl_3$ (1.0×10^{-5} M); b) half-wave reductive potentials (in V vs. Fc/Fc^+) measured in CH_2Cl_2 at a scan rate of 0.1 V s^{-1} using ferrocene as an internal potential mark; c) estimated from the onset potential of the first reduction wave and calculated according to E_{LUMO}=−(4.8+E_{onset}^{re}) eV; d) calculated according to E_{HOMO}=(E_{LUMO}−E_g) eV; e) obtained from the edge of the absorption in $CHCl_3$ solution according to E_g=(1,240/λ_{onset}).

similar trends with slightly upshifted LUMOs. The larger E_g^{opt} for **5b** is probably due to the more twisted conformation that disrupts the π-conjugation along the molecular skeleton.

2.3 Chiroptical properties

As a triple [5]helicene, the chiroptical properties of NTPH-P **5a** were further explored by circular dichroism (CD) and circular polarized luminescence (CPL) spectroscopy. As expected, the two isolated fractions showed almost identical absorption and emission properties but with perfect mirror-imaged CD and CPL signals, hinting that they are chiral isomers with opposite helicity. The simulated CD spectra of *P*,*P*,*P*- and *M*,*M*,*M*-enantiomer calculated at PBE0/6-31G(d) level are in perfect agreement with the experimental ones, suggesting the first and second fraction to be *P*,*P*,*P*- and *M*,*M*,*M*-conformer, respectively (Figure S15(b)). Enantiomerically pure NTPH-P exhibits three impressive Cotton effects in the visible region with the corresponding $|\Delta\varepsilon|$ of 239 M^{-1} cm^{-1} at 547 nm, 299 M^{-1} cm^{-1} at 491 nm, and 283 M^{-1} cm^{-1} at 423 nm, exceeding most of helicenes in the visible range. The absorption dissymmetry factor $|g_{abs}|$ for NTPH-P can reach up to 4.0×10^{-3} at 426 nm, 2.9×10^{-3} at 490 nm and 4.1×10^{-3} at 549 nm (Figure S16). Furthermore, the *P*,*P*,*P*- and *M*,*M*,*M*-enantiomers exhibited negative and positive CPL signs around 600 nm, respectively, with a luminescence dissymmetry factor $|g_{lum}|$ of 1.2×10^{-3} (Figure 5 (b)). Compared with other recently reported chiral organic molecules [31,32], the value of g_{lum} underlines the fairly high CPL activities of the enantiomers of NTPH-P. They therefore show potential to be good CPL emitters.

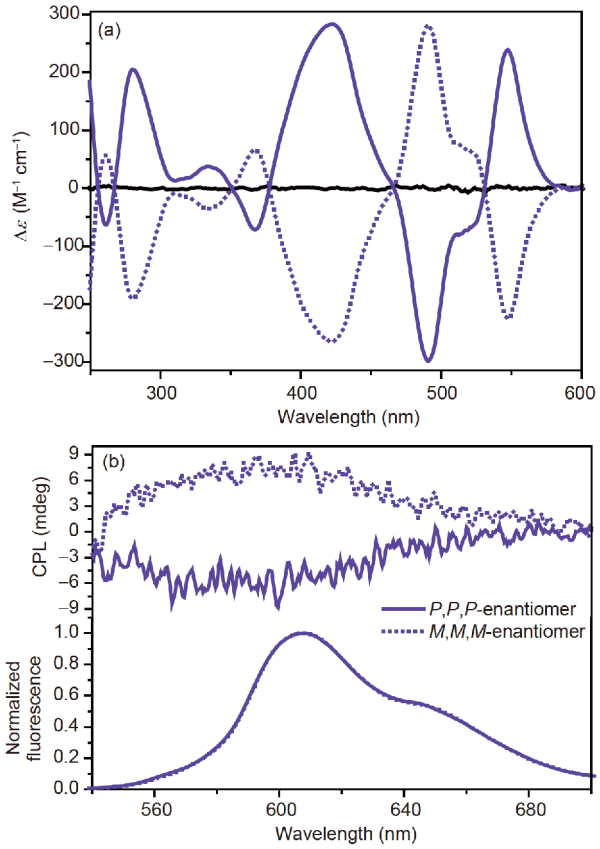

Figure 5 (a) CD spectra of racemic NTPH-P (black solid line), *P*,*P*,*P*-enantiomer (purple solid line) and *M*,*M*,*M*-enantiomer (purple dot line) in $CHCl_3$ (10^{-5} M); (b) CPL (E_x at 460 nm) and fluorescence spectra of corresponding *P*,*P*,*P*- and *M*,*M*,*M*-enantiomer in toluene (10^{-4} M) (color online).

2.4 Photovoltaic performance

Organic solar cells (OSCs) based on two stereoisomers of NTPH-P and NTPH-T1 were fabricated with an inverted structure of indium tin oxides (ITO)/ZnO/BHJ/MoO_x/Al, where the commercially available material PBDB-T was used as a donor because of its well-matched energy level and complementary absorption with NTPH [33,34]. After screening and optimizing blend ratios and processing solvents, NTPH-P:PBDB-T devices showed an excellent power conversion efficiency (PCE) of 8.11% with a fairly high open-circuit voltage (V_{OC}) of 1.00 V, a short-circuit current (J_{SC}) of 13.32 mA cm^{-2}, and a fill factor (FF) of 0.61. The devices were free of processing additives, in a way simplifying the fabrication. This increased PCE compared with TPH-based devices (PCE=6.88% and V_{OC}=0.91 V) under the same conditions is mainly owed to an increased V_{OC} for NTPH-P by the uplifted LUMO level resulting from the fused pyrrole ring at the bay region of NTPH-P. However, the other stereoisomer, NTPH-T1 based devices demonstrated a relatively poor performance of 5.24% with an inferior FF of 0.46. The current density-voltage (*J*-*V*) curves and external quantum efficiency (EQE) spectra of the optimal NTPH-P and NTPH-T1 based devices are depicted in Figure S20 and Figure 6(a). Both cells covered a wide range of photoresponse from 300 to 700 nm. Particularly, the EQE of NTPH-P based devices reached up to 78%, whereas that of NTPH-T1 based cells dropped to 63%, indicating a more efficient conversion of photo-to-current for NTPH-P:PBDB-T cells. The respective calculated J_{SC} integrated from the EQE spectra were 12.40 and 10.86 mA cm^{-2} for NTPH-P and NTPH-T based devices, well agreed with the measured ones from *J*-*V* plots.

To explore the reasons causing the different performances between the diastereoisomers, the surface morphologies of the bulk heterojunction (BHJ) films were probed by atomic force microscopy (AFM). Obvious differences were observed between NTPH-P and NTPH-T1 based blend films. As shown in Figure 6(b), larger domain size with apparent clumps was seen for NTPH-T1 blend film, along with a root-mean-square (RMS) roughness of 2.47 nm. By contrast, the NTPH-P blend film exhibited a much smooth and uniformed surface texture with smaller phase separation size and a RMS

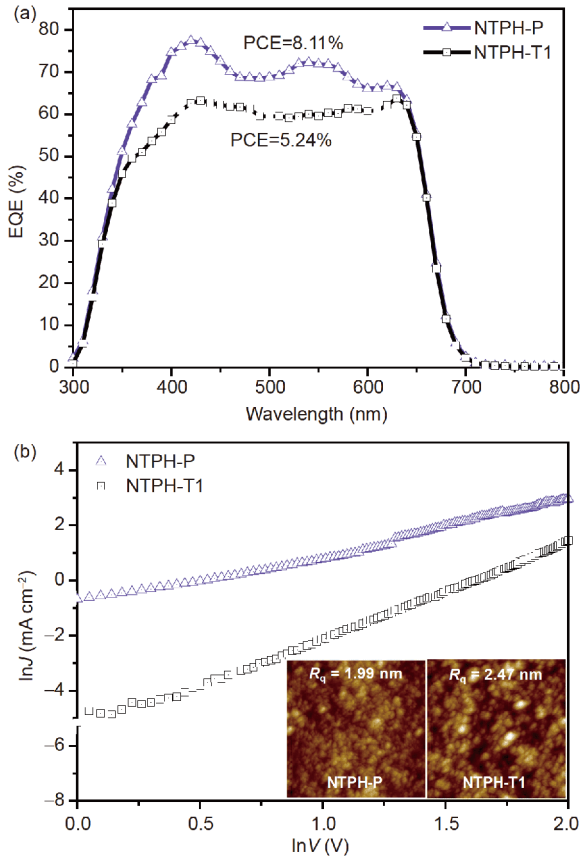

Figure 6 (a) EQE spectra of NTPH-P and NTPH-T1 based solar cells and (b) plots of ln$J$ vs. ln$V$ obtained from the electron-only devices. Insets show their AFM images of optimal blend films (color online).

of 1.99 nm. The better compatibility for NTPH-P:PBDB-T blend film can favor the exciton diffusion and separation, and thus induce a better J_{SC} and FF.

We further measured the charge transfer properties in the optimal blend films via the space-charge-limited current (SCLC) method with the device configuration of ITO/ZnO/BHJ/Al and ITO/PEDOT:PSS/BHJ/Al for electron and hole mobilities, respectively. As shown in Figure 6(b) and Figure S21, the electron mobility was determined to be 6.09×10^{-6} cm^2 V^{-1} s^{-1} for the NTPH-P:PBDB-T blend film, but collapsed to 4.40×10^{-8} cm^2 V^{-1} s^{-1} for the NTPH-T1:PBDB-T. The two orders of magnitude enhanced electron mobility and a superiorly balanced hole and electron mobility ratio (μ_h/μ_e=5) can lead to a higher J_{SC} and FF for NTPH-P based devices.

3 Conclusions

In conclusion, a C_2-symmetric triple [5]helicene based on *N*-annulated triperylene hexaimide (NTPH) was designed and synthesized by a combination of multiple helicities and asymmetric decoration strategy. Aided by experimental and theoretical support, we detailed the structural isomerization and photo-physical properties between two diastereoisomers (NTPH-P and NTPH-T1), in which **5a** and **5b** were assigned to propeller and twisted conformation, respectively. Then we succeeded in chiral resolution of NTPH-P and further clarified the chiroptical properties of ground and excited state by CD and CPL spectra. Fairly high values for $|g_{abs}|$ of up to 4.1×10^{-3} and $|g_{lum}|$ of 1.2×10^{-3} were obtained. These preeminent chiral characteristics of NTPH-P suggest a potential application in chiroptical electronics, for instance, as CPL emitter. In addition, the conformational distinction endowed NTPH-P based devices with a better morphology and carriers mobilites, showing superior photovoltaics performance with a PCE of up to 8.11%.

Acknowledgements We thank Dr. Junfeng Xiang at the Institute of Chemistry, Chinese Academy of Sciences for his fruitful suggestions of NMR mearsurements. We thank Dr. Jianlei Han and Prof. Dr. Pengfei Duan for their assistance with CPL spectra measurements and analyses. This work was supported by the National Natural Science Foundation of China (21790361, 21734009), the National Key R&D Program of China (2017YFA0204701), the Youth Innovation Promotion Association of Chinese Academy of Sciences (2017048), and DFG within TRR 61.

Conflict of interest The authors declare that they have no conflict of interest.

Supporting information The supporting information is available online at http://chem.scichina.com and http://link.springer.com/journal/11426. The supporting materials are published as submitted, without typesetting or editing. The responsibility for scientific accuracy and content remains entirely with the authors.

1 Ball M, Zhong Y, Wu Y, Schenck C, Ng F, Steigerwald M, Xiao S, Nuckolls C. *Acc Chem Res*, 2015, 48: 267–276
2 Rickhaus M, Mayor M, Juríček M. *Chem Soc Rev*, 2016, 45: 1542–1556
3 Wu YT, Siegel JS. *Chem Rev*, 2006, 106: 4843–4867
4 Wang XY, Yao X, Müllen K. *Sci China Chem*, 2019, 62: 1099–1144
5 Zheng C, Zhu J, Yang C, Lu C, Chen Z, Zhuang X. *Sci China Chem*, 2019, 62: 1145–1193
6 Zhang Z, Ma W, Xu B, Zhou X, Wang C, Xie Z, Liu L, Ma Y. *Sci China Chem*, 2018, 61: 192–199
7 Pun SH, Miao Q. *Acc Chem Res*, 2018, 51: 1630–1642
8 Shen Y, Chen CF. *Chem Rev*, 2012, 112: 1463–1535
9 Dhbaibi K, Favereau L, Crassous J. *Chem Rev*, 2019, 119: 8846–8953
10 Gingras M. *Chem Soc Rev*, 2013, 42: 968–1006
11 Gingras M, Félix G, Peresutti R. *Chem Soc Rev*, 2013, 42: 1007–1050
12 Gingras M. *Chem Soc Rev*, 2013, 42: 1051–1095
13 Josse P, Favereau L, Shen C, Dabos-Seignon S, Blanchard P, Cabanetos C, Crassous J. *Chem Eur J*, 2017, 23: 6277–6281
14 Lin WB, Li M, Fang L, Chen CF. *Chin Chem Lett*, 2018, 29: 40–46
15 Li C, Yang Y, Miao Q. *Chem Asian J*, 2018, 13: 884–894
16 Reger D, Haines P, Heinemann FW, Guldi DM, Jux N. *Angew Chem Int Ed*, 2018, 57: 5938–5942
17 Wang XY, Narita A, Zhang W, Feng X, Müllen K. *J Am Chem Soc*, 2016, 138: 9021–9024
18 Pradhan A, Dechambenoit P, Bock H, Durola F. *Angew Chem*, 2011, 123: 12790–12793
19 Saito H, Uchida A, Watanabe S. *J Org Chem*, 2017, 82: 5663–5668
20 Bennett MA, Kopp MR, Wenger E, Willis AC. *J Organomet Chem*, 2003, 667: 8–15
21 Fujikawa T, Segawa Y, Itami K. *J Am Chem Soc*, 2016, 138: 3587–

3595
22 Arslan H, Uribe-Romo FJ, Smith BJ, Dichtel WR. *Chem Sci*, 2013, 4: 3973–3978
23 Meng D, Liu G, Xiao C, Shi Y, Zhang L, Jiang L, Baldridge KK, Li Y, Siegel JS, Wang Z. *J Am Chem Soc*, 2019, 141: 5402–5408
24 Kato K, Segawa Y, Scott LT, Itami K. *Angew Chem*, 2018, 130: 1351–1355
25 Wang Y, Yin Z, Zhu Y, Gu J, Li Y, Wang J. *Angew Chem Int Ed*, 2019, 58: 587–591
26 Zhu Y, Guo X, Li Y, Wang J. *J Am Chem Soc*, 2019, 141: 5511–5517
27 Meng D, Fu H, Xiao C, Meng X, Winands T, Ma W, Wei W, Fan B, Huo L, Doltsinis NL, Li Y, Sun Y, Wang Z. *J Am Chem Soc*, 2016, 138: 10184–10190
28 Freeman AW, Urvoy M, Criswell ME. *J Org Chem*, 2005, 70: 5014–5019
29 Ma Z, Fu H, Meng D, Jiang W, Sun Y, Wang Z. *Chem Asian J*, 2018, 13: 918–923
30 Hu Y, Wang XY, Peng PX, Wang XC, Cao XY, Feng X, Müllen K, Narita A. *Angew Chem Int Ed*, 2017, 56: 3374–3378
31 Sánchez-Carnerero EM, Agarrabeitia AR, Moreno F, Maroto BL, Muller G, Ortiz MJ, de la Moya S. *Chem Eur J*, 2015, 21: 13488–13500
32 Han J, Guo S, Lu H, Liu S, Zhao Q, Huang W. *Adv Opt Mater*, 2018, 6: 1800538
33 Qian D, Ye L, Zhang M, Liang Y, Li L, Huang Y, Guo X, Zhang S, Tan Z', Hou J. *Macromolecules*, 2012, 45: 9611–9617
34 Huo L, Liu T, Sun X, Cai Y, Heeger AJ, Sun Y. *Adv Mater*, 2015, 27: 2938–2944